

## Development of fluxgate magnetometers and applications to the space science missions

A. Matsuoka<sup>1</sup>, M. Shinohara<sup>2</sup>, Y.-M. Tanaka<sup>3</sup>, A. Fujimoto<sup>1</sup>, and K. Iguchi<sup>4</sup>

<sup>1</sup>*Institute of Space and Astronautical Science, Japan Aerospace Exploration Agency, Japan*

<sup>2</sup>*Kagoshima National College of Technology, Japan*

<sup>3</sup>*National Institute of Polar Research, Japan*

<sup>4</sup>*The Graduate University for Advanced Studies, Department of Space and Astronautical Science, Japan*

Magnetic field is one of the essential physical parameters to study the space physics and evolution of the solar system. There are several methods to measure the magnetic field in the space by spacecraft and rockets. Fluxgate magnetometer has been most generally used out of them because it measures the vector field accurately and does not need much weight and power budgets. When we try more difficult missions such as multi-satellite observation, landing on the celestial body and exploration in the area of severe environment, we have to modify the magnetometer or develop new techniques to make the instrument adequate for those projects. For example, we developed a 20-bit delta-sigma analogue-to-digital converter for MGF-I on the BepiColombo MMO satellite, to achieve the wide-range ( $\pm 2000$  nT) measurement with good resolution in the high radiation environment. For further future missions, we have examined the digitalizing of the circuit, which has much potential to drastically reduce the instrument weight, power consumption and performance dependence on the temperature.

**Key words:** Magnetometer, magnetic field, space science.

### 1. Magnet Fields in the Space

The magnetic fields in the space are classified into three types according to the generation sources. One is the field having the source inside or on the surface of celestial body, e.g., the Sun, planets and satellites in the solar system. In the cases of the Earth, Mercury and outer planets than Mars, magnetic dynamo is working in the liquid core, and the magnetic moment is placed at the center of the planets. The area where the magnetic field is effective spreads in the range of the planetary scale and is called “magnetosphere”. Meanwhile the Moon and Mars do not have significant magnetic moment. There are weakly “magnetized” parts on the surface.

The second category is the magnetic field caused by the electric current carried by plasma. For example, in the Earth’s magnetosphere, magnetic field lines coming from the Antarctic region or going to the Arctic region are extended in the night direction. This configuration is represented by the summation of the magnetic fields generated by the Earth’s intrinsic moment and the field along the Sun-Earth direction. The latter field is maintained by the electric current flowing from dawn to dusk in the plasmashet.

The third is the inductive field. One of the Maxwell’s equation,  $\text{rot}\mathbf{E} = -(\partial\mathbf{B})/(\partial t)$ , represents that the rotation of the electric field is accompanied by the temporal change of the magnetic field.

The time scale of the magnetic fields having the source inside or on the surface of the planets is substantially long, although they are not perfectly constant. The polarity of the earth magnetic dipole is known to have changed on the time scale of million years. The magnetic fields generated by the

electrical currents vary on the relatively short time scale, although the frequency and amplitude depend on the source phenomena. The time and spatial scales of the inductive fields, those are often observed as waves propagating in the plasma, are generally further small.

### 2. Aims of the Magnetic Field Measurement by Spacecraft and Rockets

There are several purposes to measure the magnetic fields in the space by spacecraft and rockets. Some of them are investigations in the nature science field, and the others are related with the space technology. (1) Investigation of the interior structure and surface condition of the Sun, planets and moons by measuring the magnetic field generated in these celestial bodies. It helps our comprehension about the evolution of the celestial bodies and the solar system. (2) Interpretation of the plasma motion in the space. When we study the space plasma, we always need the simultaneous magnetic field data to interpret the plasma data, because the magnetic field controls the motion of the charged particles. (3) Investigation of the inductive or time-varying phenomena in the space. The energy transfer in the space plasma is often accompanied by the burst phenomena (e.g. magnetic substorm), steep discontinuities (e.g. interplanetary shock), and plasma waves. They are characterized by the rapid temporal and spatial variations of the magnetic field. (4) Determination of the attitude of the spacecraft and rockets. When the magnetic field direction is well modeled in the absolute coordinate (e.g. in the neighbor region around the Earth), the measured magnetic field can be used to determine the attitude of the spacecraft and rockets. (5) When spacecraft orbits at low altitudes around the Earth, its attitude may be controlled by the force working from the geomagnetic field to the satellite in which magnetic moment is gener-

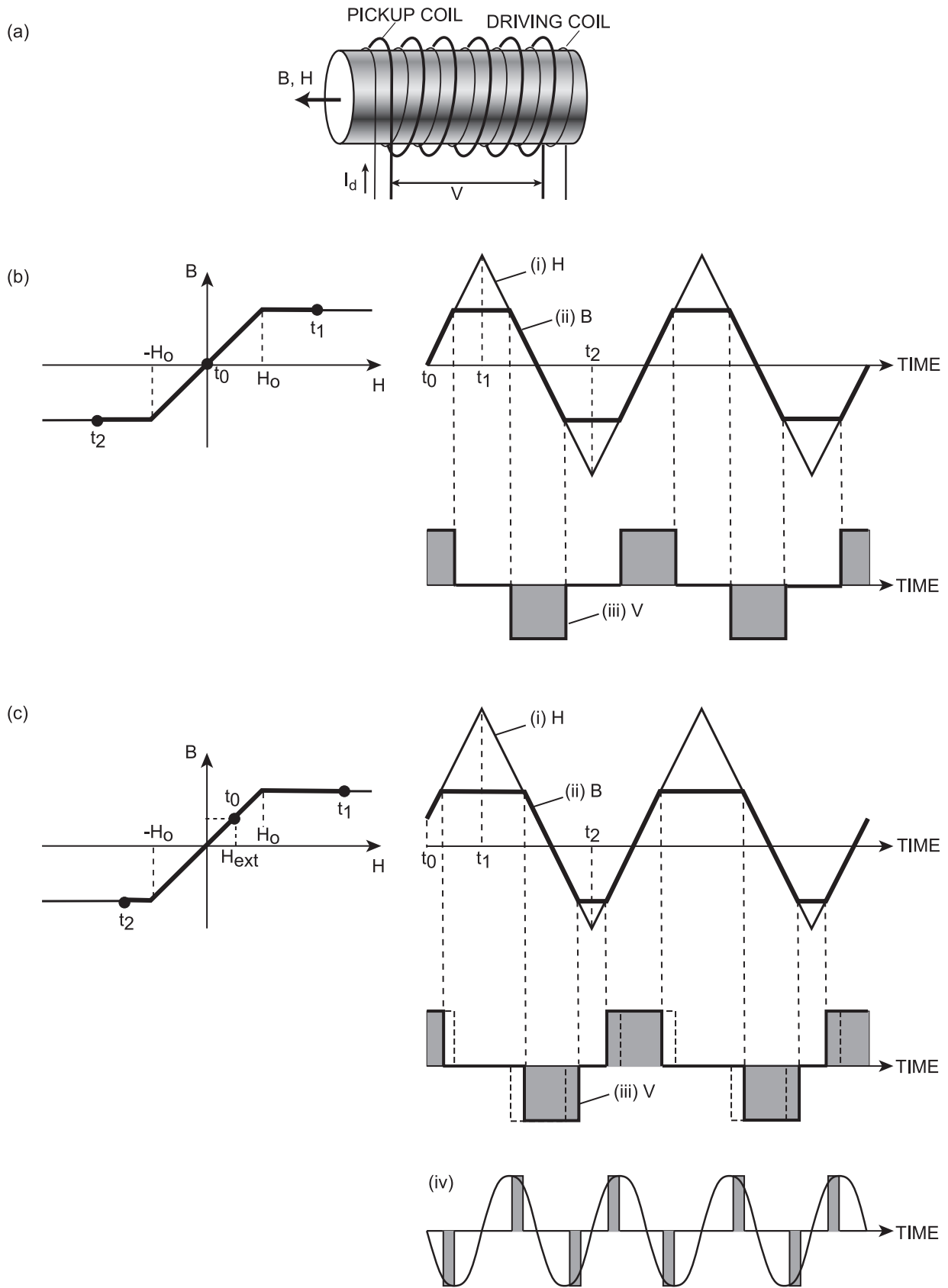


Fig. 1. Schematic drawings to explain the principle of the fluxgate magnetometer with a single-rod core. (a) A bar-shape core and two coils (driving and pickup coils) wound around it. (b) Plots of the magnetic field  $H$ , flux density  $B$  in the core and voltage generated in the pickup coil  $V$  when there is no external field aligned the coil axis. (c) Plots of  $H$ ,  $B$  and  $V$  when there is finite external field  $H_{ext}$  aligned the coil axis. (iv) is the difference in the voltage  $V$  between the cases (b) and (c).

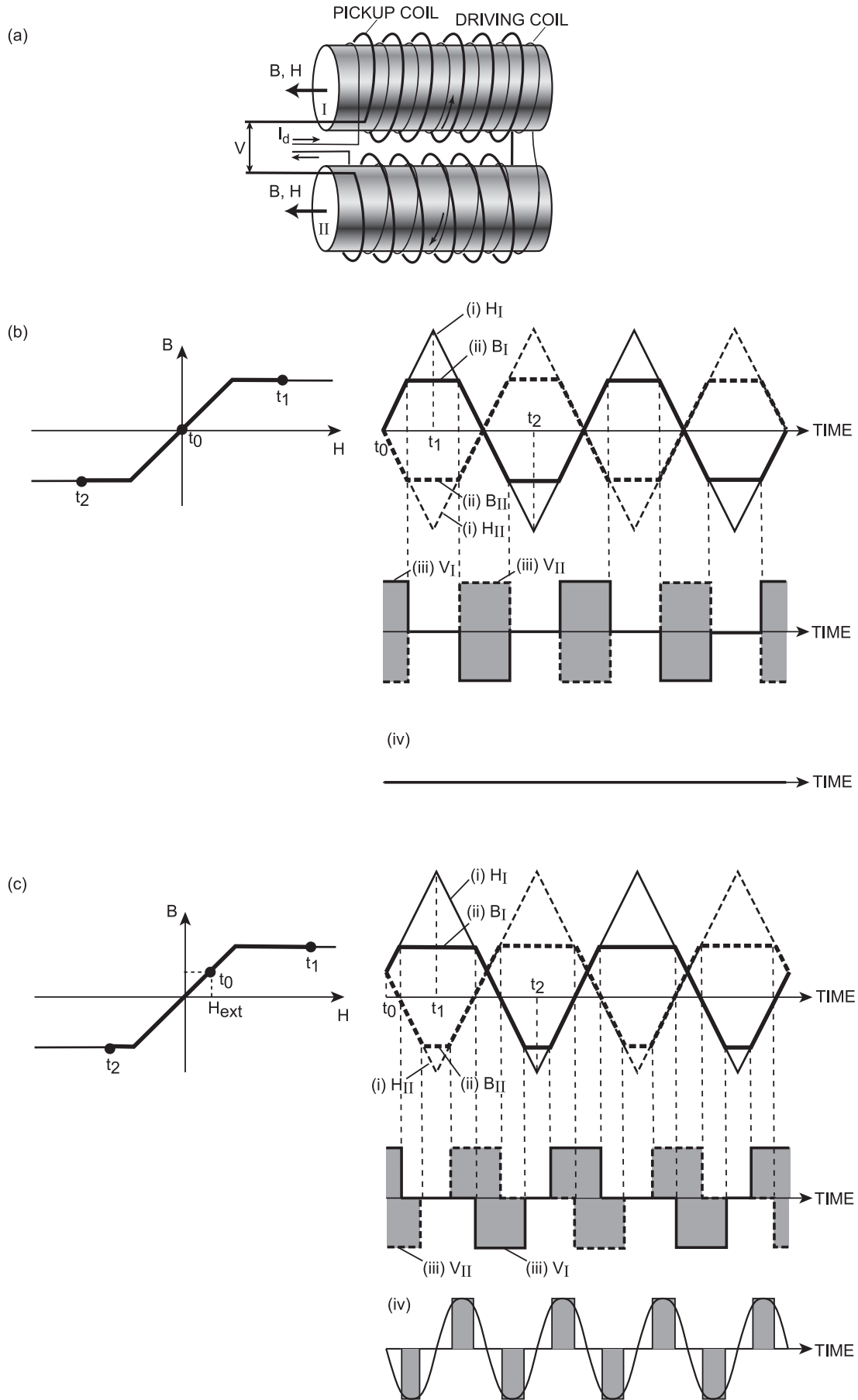


Fig. 2. Schematic drawings to explain the principle of the fluxgate magnetometer with double-rods core. The format is same as Fig. 1. The suffix I and II denote the cores I and II respectively.

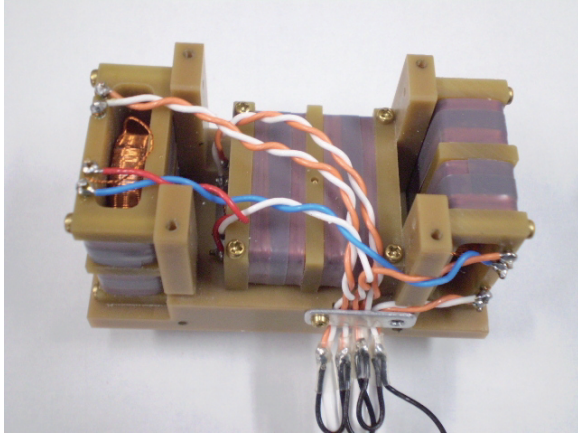


Fig. 3. Photo of the sensor unit of the fluxgate magnetometer, DFG, which flew on the S-310-38 sounding rocket.

ated. For the precise attitude control, the geomagnetic field at the satellite position should be measured.

### 3. Techniques to Measure Magnetic Field

Although there are plenty of methods to measure magnetic field in general terms, the proper methods for the in-situ measurement in the space are limited to several. The intensity range of the field where spacecraft may reach is from 1 to  $10^5$  nT at most. The most intense magnetic field measured by spacecraft was approximately 1 gauss ( $10^5$  nT) during the fly-by of Jupiter by Pioneer 11 (Acuna and Ness, 1976, 1980). Efforts have been made to improve the measurement accuracy of such a relatively weak magnetic field.

The methods to measure the magnetic field in the space are classified into scalar measurement and vector measurement. As magnetometers to measure the intensity of the field, proton free precession and Rubidium vapor self-oscillating types were often used for the spacecraft experiments in 1960's and 1970's (Ness, 1970). To improve the sampling frequency and sensitivity of the proton free precession magnetometer, Overhauser effect proton magnetometer was developed and adopted for Ørsted and CHAMP satellites (Primdahl, 1998). Another type of the optically-pumped magnetometer than the Rubidium vapor self-oscillating type, helium magnetometer was installed on Cassini to explore the Saturn and its satellites (Kellock, 1996; Dougherty *et al.*, 2004).

Instruments for the vector field measurement are classified into DC and AC magnetometers. Most common type of the magnetometer for the DC vector measurement is fluxgate magnetometer. The history, principle and practical design examples of the fluxgate magnetometer will be shown in detail in the following sections. The other type of the DC vector magnetometer is helium vector magnetometer. It has the basically same design as the helium scalar magnetometer which was already mentioned, except three-axis orthogonal helmholtz-coil is wound around the sensor to measure the vector field (Ness, 1970).

Search-coil magnetometers and loop antennas are used to measure the magnetic-field variations of frequencies at around and higher than 1 Hz (Gurnett, 1998). Search-coil

sensor is a coil with high-permeability metal core, and loop antenna is an air-core coil. Whereas the fluxgate magnetometer is an active sensor, as will be explained in the next section, the search-coil and loop antenna are passive sensors. The induced voltage in the coil or loop by the field variation is detected, and interpreted as the time differential of the magnetic flux.

To achieve the objectives we have described in the previous section, both intensity and direction of the magnetic field should be measured. For the projects where the magnetic field measurement is required, magnetometers measuring the vector DC field (usually fluxgate magnetometer) have been used. When the field intensity should be precisely determined to achieve the mission objectives, the magnetometers for the scalar measurement were installed together. For example, on MAGSAT a Cesium vapor scalar magnetometer was installed with a fluxgate vector magnetometer (Acuna *et al.*, 1978), and on Ørsted an Overhauser scalar magnetometer was with a fluxgate magnetometer (Nielsen *et al.*, 1995)

## 4. Fluxgate Magnetometer

### 4.1 History

Fluxgate magnetometer is one of the instruments which have been installed on spacecraft and rockets since the early days of the space exploration in the late 1950's (Gordon and Brown, 1972). The first spacecraft on which a fluxgate magnetometer was installed was Sputnik III launched in 1958 (Ness, 1970). Since then most of the important findings in the fields of planetary/satellite magnetism and plasma physics have been carried by the fluxgate magnetometers.

### 4.2 Principle

The basic elements composing the fluxgate magnetometer sensor are metal core, driving coil, and pickup coil. Ferromagnetic materials of high initial permeability are used as the sensor core. Permalloy, a kind of nickel-iron alloy, has been most commonly used.

In this chapter we will make a conceptual explanation of the principle of the fluxgate magnetometer. Primdahl (1979) and some other papers explain the principle of the fluxgate magnetometer by more analytic expressions.

Now we consider a simple fluxgate system in which two coils, driving and pickup coils, are wound around a bar-shape core (Fig. 1(a)). At first we assume that there is no external magnetic field. The ferromagnetic core has the characteristics that the flux density  $B$  inside the core is approximately proportional to the magnetic field  $H$  if  $H$  is not intense, while  $B$  is saturated and constant for intense  $H$  (Fig. 1(b)). We define  $\pm H_0$  as the magnetic field when  $B$  reaches the saturation. Electric current is provided to the driving coil and  $H$  is given to the core in the direction along the coil axis. When  $H$  changes periodically, as illustrated in Fig. 1(b),  $B$  changes in the similar manner to  $H$  for weak  $H$ , but is constant for intense  $H$  outside  $\pm H_0$ . (Note that the triangle wave form in the figure is drawn for the schematic expression. The actual wave forms used for the magnetometers are different.) Voltage is induced in the pickup coil while  $B$  changes, and no voltage exist for the constant  $B$ .

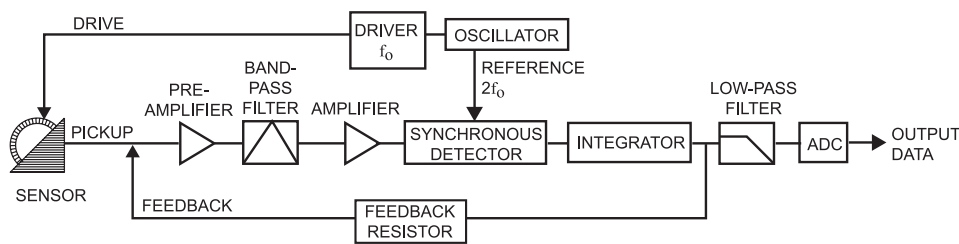


Fig. 4. Simplified diagram of the fluxgate magnetometer.

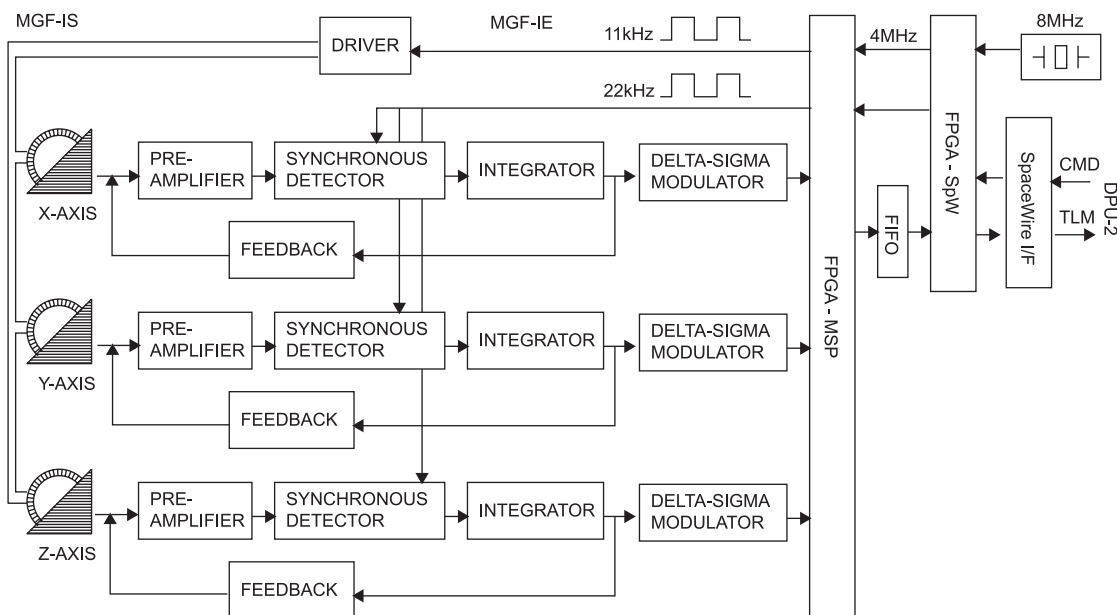


Fig. 5. Block diagram of MGF-I, the fluxgate magnetometer for BepiColombo MMO.

Next we consider the condition that there is an external magnetic field,  $H_{ext}$ , along the coil axis. When we provide the electric current to the driving coil in the same manner as the no external-field case, the total magnetic field  $H$  given to the core has a bias  $H_{ext}$  (Fig. 1(c)). It changes the duration, start and end timings of the period when  $B$  is saturated. In Fig. 1(c), (iv) schematically shows the difference of the induced voltage between two cases (no external field and finite external field). Its frequency is the twice (secondary harmonic) of the frequency of the current provided to the driving coil. It indicates that, when there is an external field, the induced voltage in the pickup coil has the component of the twice frequency of the driving current. The amplitude is approximately proportional to the external field strength.

The most serious problem of this single-rod type sensor is that, in the induced voltage in the pickup coil, the secondary harmonic component is much less intense compared with the primary component. Next we consider a double-rods type sensor as illustrated in Fig. 2. We use two bar-shape cores, I and II, placed in parallel to each other. The pickup coils are wound in the same direction for I and II, but driving coils are in the opposite directions. When there is no external field along the coil axis, the induced voltage in the pickup coil wound around the core I,  $V_I$ , balances with the

induced voltage in the pickup coil wound around the core II,  $V_{II}$ . Therefore no signal appears in the voltage between the ends of the serially connected pickup coils. When there is an external field along the core axis, only the signal of secondary harmonic component appears in the voltage of the pickup coil, since the primary components are balanced to each other between I and II again. By measuring the amplitude and phase of the secondary harmonic component, it is possible to know the intensity and polarity of the external magnetic field.

### 4.3 Practical design

Ring-shape cores are often used in the fluxgate magnetometers for spacecraft and rocket experiments. The ring-shape core may be considered as the improved one of the double-rod core by connecting the ends. The driving coil is wound along the circumference of the ring, and two pickup coils are modified into one coil wound around the whole ring-shape core.

Figure 3 shows the photo of a sensor unit of the fluxgate magnetometer which flew on the JAXA sounding rocket S-310-38. It consists of three one-axis sensors and a sensor base. The one-axis sensors are installed on the base to make the measurement axes perpendicular one another to measure the orthogonal three components.

Figure 4 shows the simplified block diagram of the flux-

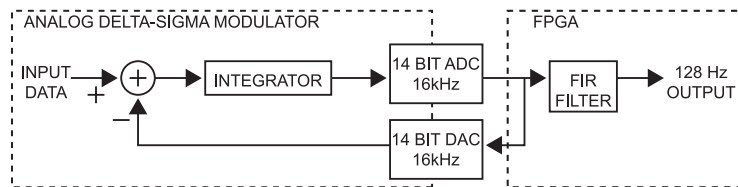


Fig. 6. Diagram of the delta-sigma analogue-to-digital converter for MGF-I.

Table 1. Characteristics of MGF-I for BepiColombo MMO.

Item	Value/Description	Note
Sensor core	20 mm $\phi$ ring core of nickel-molybdenum Permalloy	
Driving frequency	11 kHz	
Noise density at 1 Hz	7.7–8.9 nT/Hz <sup>1/2</sup>	Engineering model
RMS in 0.1–10 Hz frequency range	33.5–37.3 pT	Engineering model
Dynamic range	$\pm 2000$ nT	
Resolution	20 bits (1 digit = 4 pT)	
Sampling frequency	128 Hz	
Weight		
Electric circuit board	414 g	Nominal
Sensor	118 g	Flight model
Power consumption	2.17 W	Nominal

gate magnetometer. The driving circuit provides the current to the driving coil. The sensing circuit at first amplifies and band-passes the secondary-harmonic component in the signal from the pickup coil. The amplitude of the amplified signal is detected, being synchronized with the driving signal. The output value represents the intensity and polarization of the external magnetic field.

For the wide measurement range and better performance, “null method” is often employed by addition of a feedback coil wound along the same axis as the pickup coil. The output from the synchronous detector is integrated, and current which is proportional to the result is provided to the feedback coil. The current changes until the generated field at the sensor position balances with the external field. When the balance is established, the output from the integrator is proportional to the external field, and the coefficient is decided by the resistor between the integrator and feedback coil. By selecting the resistor according to the field intensity, it is possible to tune the dynamic range of the measurement. To reduce the weight, pickup and feedback coils are sometimes put together.

## 5. Fluxgate Magnetometer (MGF-I) Developed by ISAS/JAXA for BepiColombo MMO

### 5.1 BepiColombo project and MGF-I

BepiColombo is a JAXA-ESA joint mission to explore Mercury (Benkhoff *et al.*, 2010). It consists of two satellites, Mercury Magnetospheric Orbiter (MMO) and Mercury Planetary Orbiter (MPO), and is planned to be launched in 2014. Both satellites have two sets of fluxgate magnetometer respectively. One of the magnetometers for MMO is MGF-I, which is developed by Institute of Space and Astronautical Science (ISAS), Japan Aerospace Exploration Agency (JAXA) and co-workers in Japan. The other magnetometer is MGF-O, which is manufactured by

the Institut fuer Weltraumforschung (IWF) of the Austrian Academy of Sciences and the Institut fuer Geophysik und extraterrestrische Physik (IGEP) of the Technical University in Braunschweig, Germany (Baumjohann *et al.*, 2010). MMO has two extensible MASTs (5-meter length) to separate the magnetometer sensors from the spacecraft body. The MGF-O sensor is installed at the tip of one of the MASTs, and MGF-I sensor is on the same MAST at the 2.9m distance from the root. The other MAST is for the search-coil magnetometers.

Instruments for MMO are required to strictly limit the mass and power consumption to reduce the total spacecraft mass and the heat generation. Moreover they should be tolerant of the severe radiation and thermal environment at Mercury. The required tolerance depends on the installed location and thermal condition inside the spacecraft. The expected total dose at the position of the MGF-I electronics without chassis is approximately 70 krad at the end of the mission. As for the thermal environment, MGF-I electronics is required to have the nominal performance in the temperature range from  $-30$  to  $60$  degrees centigrade. Because the extensible MAST is thermally isolated from the MMO spacecraft, the temperature of the MGF-I sensor is expected to range from  $18$  to  $154$  degrees centigrade, which is higher and wider than the temperatures inside the spacecraft body.

### 5.2 Design and performance of MGF-I

Figure 5 shows the block diagram of MGF-I, and Table 1 shows the characteristics. The design of MGF-I is based on the fluxgate magnetometers manufactured for previous Japanese space-science missions, e.g. Geotail (magnetospheric observation) and Nozomi (Mars exploration). Meanwhile some technological elements were newly developed for MGF-I to make it tolerant of the severe environment at Mercury, and meet the requirements to the MMO instruments.

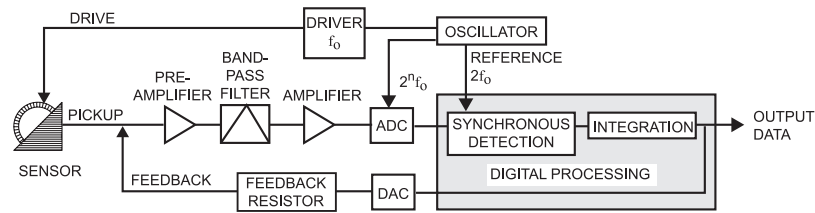


Fig. 7. Simplified diagram of the digital-type fluxgate magnetometer.

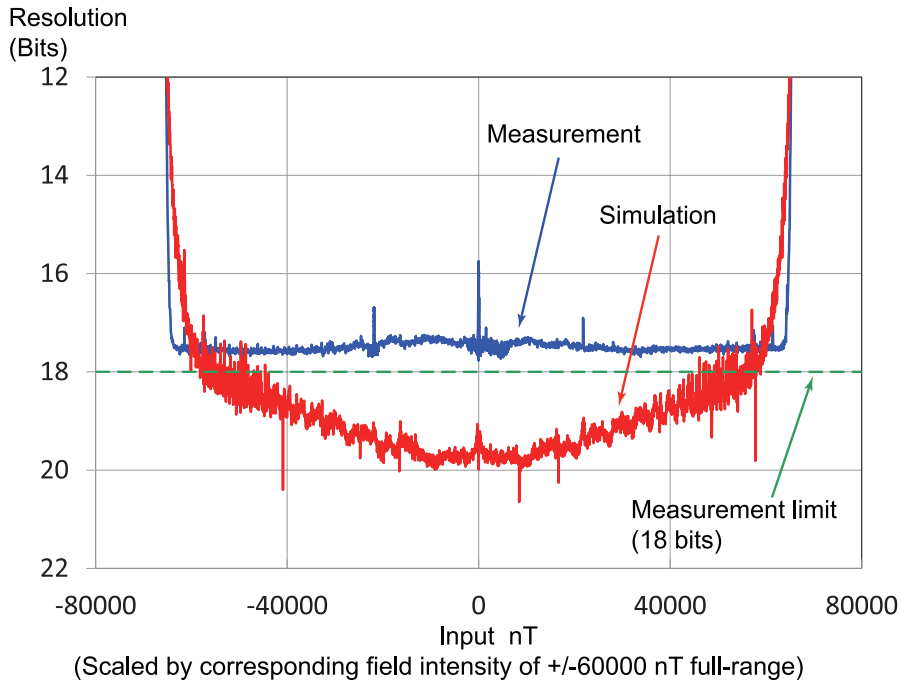


Fig. 8. Noise in the output data of the bread-board model of the high-bit Digital-to-Analogue Converter (DAC). The horizontal axis is scaled by the input to the DAC while the vertical axis is scaled by the resolution expressed by bits.

In the early phase of the examination of the MMO design, the temperature of the sensor was anticipated to be raised up to around 200 degrees centigrade. Therefore a kind of ceramics, Photovee (tolerant of high temperature up to 1000 degrees centigrade) is used for the pickup/feedback coil bobbin and sensor base.

The expected possible maximum field intensity MMO will observe in the orbit around Mercury is 1000 nT. The dynamic range  $\pm 2000$  nT is defined for the measurement with good margin. When the analogue output is converted to the digital signal with 14-bit resolution, which would be the best one by commercial parts tolerant of the MMO radiation environment, the data resolution would be 0.25 nT. We need additional smaller dynamic range for the precise measurement of small fields. It would be  $\pm 64$  nT if we need 8 pT resolution, although precise measurement of the field larger than 64 nT is impossible. Moreover, when the intensity of the magnetic field increases rapidly, e.g. at the crossing of the interplanetary shock front, the data are possibly lost during the switching of the feedback resistor. If a high bit Analogue-to-Digital Converter (ADC) is available, measurement of  $\pm 2000$  nT with good resolution would be possible and these problems would be solved. In the following section, one of new technological elements developed

for MGF-I, radiation-tolerant 20-bit ADC circuit, is shown in detail.

### 5.3 Radiation-tolerant 20-bit analog-to-digital converter

Figure 6 shows the block diagram of the delta-sigma analogue-to-digital converter we have developed. It consists of analogue circuit of delta-sigma modulation, a 14-bit ADC, 14-bit Digital-to-Analogue Converter (DAC) and Finite Impulse Response (FIR) filter in the FPGA. The analogue delta-sigma modulator and the ADC generate 16 kHz delta-sigma modulated data. The modulated data is fed back and subtracted from the next input data. The FPGA filters the digitized data and outputs the 128-Hz digital data of 20-bit resolution. All parts used in this ADC system have the radiation tolerance of 100 krad.

The performance of the delta-sigma modulator and the FIR filter by FPGA were designed based on the simulations. The frequency characteristics of the delta-sigma ADC has the cut-off ( $-3$  dB) at 52 Hz and the time delay is constant (half length of the FIR filter window) up to 128 Hz.

The linearity of the delta-sigma ADC of the MGF-I engineering model was experimentally examined. The linearity errors of the full ranges ( $\pm 2000$  nT) of three axes are smaller than 0.008%, corresponding to 0.32 nT, and satis-

## Requirements to future magnetometers for space-science missions

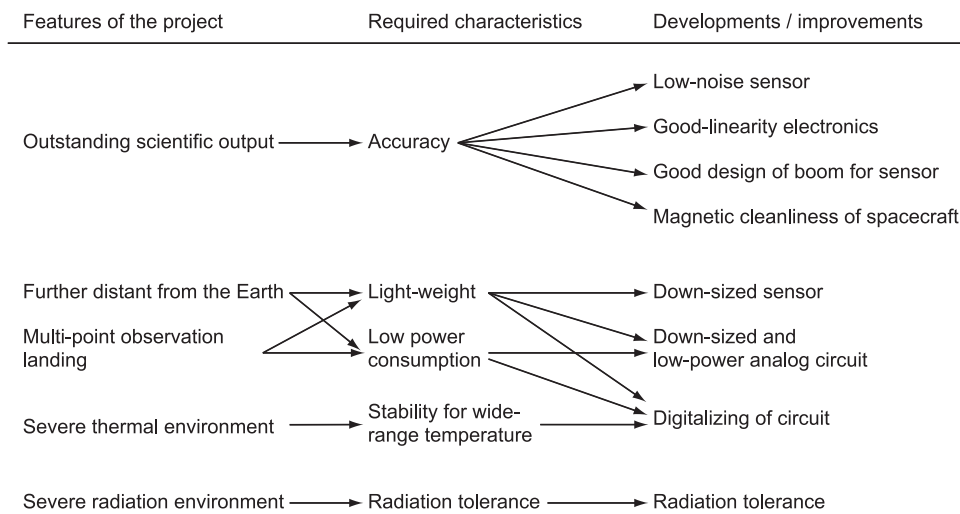


Fig. 9. Diagram to show the relationship between the features of the future space science projects and required developments/improvements to the magnetometers.

fies the target linearity error of MGF-I, 0.01%.

To evaluate the noise of the same delta-sigma ADC, the standard deviation (STD) in the output data from the ADC was examined. The noise STD has the minimum (less than 1 digit) at the zero input, and increases with increasing input intensity up to  $\sim 2$  digits. 2 digits noise corresponds to the 8 pT magnetic field noise which is much less than the noise caused by the sensor (see Table 1).

## 6. Development of Digital-Type Fluxgate Magnetometer

### 6.1 Basic concept of digital-type fluxgate magnetometer

One of the disadvantages of the conventional fluxgate magnetometers is that the performance of analogue electric parts generally has dependence on the temperature. Determination of the measurement offset, output value in the null field, by the in-flight calibration is important to achieve the accurate absolute field measurement. For the in-flight calibration, data of the magnetometer for substantial interval are accumulated and analyzed statistically. The offset should be stable to determine the offset value accurately. When we send spacecraft to the places where the instrument temperature significantly changes, such temperature dependence would make the precise field measurement difficult. One of the means to reduce the temperature dependence is digitalizing of the electrical circuit. Another advantage of the digitalizing of the circuit is that it has much potential to reduce the weight and power consumption of the magnetometer. In the future projects of multi-satellites, landers and planetary orbiters, the available resources for the spacecraft payload will be further severely restricted. For the magnetometers for such projects, both weight and power consumption will be strongly required to be reduced.

In the circuit of the digital-type fluxgate magnetometer, as illustrated in Fig. 7, the amplified pick-up analogue signal is converted into digital by ADC. The processing part in-

cluding synchronous detection and integration is composed by digital processors. The digital value for the feedback is converted into analogue by DAC, which provides the electric current to the feedback coil.

### 6.2 Practical developments of digital-type fluxgate magnetometers

Some models of the digital-type magnetometer for spacecraft have been developed for Astrid-2 (Pedersen *et al.*, 1999), ROSETTA orbiter (Glassmeier *et al.*, 2007), ROSETTA lander (Auster *et al.*, 2007), and THEMIS (Auster *et al.*, 2008). MGF-O for BepiColombo MMO has also the digital-type design similar to that for THEMIS (Baumjohann *et al.*, 2010). In Japan, independently from the European developments, we have developed a digital-type fluxgate magnetometer. The first model flown in the space is DFG for the S-310-38 sounding rocket launched in 2008. 16-bit ADC and 16-bit DAC were used for the signal conversion. The dynamic range is  $\pm 60000$  nT and the sampling frequency is 200 Hz.

Because space-use highly-reliable commercial 16-bit DAC is not available now, we are developing a high-bit DAC circuit by the delta-sigma technique we used in the ADC for BepiColombo MMO MGF-I. Figure 8 shows the plot of the standard deviation of the noise of the bread-board model DAC. The noise is confirmed to be much smaller than 17-bit resolution for most input values in the dynamic range  $\pm 60000$  nT. The noise calculated by the simulation of the ideal delta-sigma behavior is plotted in the same panel, and less than the measurement. Considering the limit of the measurement instrument (the ADC used to measure the output from the delta-sigma DAC has the noise corresponding to 18-bit resolution), we may presume that the real noise in the output from the delta-sigma DAC is smaller than the measurement result. The linearity error of the bread-board model DAC is less than 0.006% corresponding to 14-bit resolution, which is comparable to the measurement error 0.005%.

A flight model using the delta-sigma DAC is ready to fly on the S-310-40 sounding rocket. The basic characteristics are same as DFG for S-310-38; the dynamic range is  $\pm 60000$  nT and the sampling frequency is 200 Hz. In this model the newly-developed delta-sigma DAC is used for one of the three axes. For other two axes, the circuit and logical design is almost same as DFG for S-310-38, in which commercial 16-bit DACs are used in all three axes. In the functional test, the standard deviation of the noise in the output value from DFG for S-310-40 was found to be less than 1 digit of DAC (2 nT) in all three axes.

## 7. Required Developments for Future Magnetometers

Figure 9 shows the diagram of the subjects required to the magnetometers in the future missions. If the mass and power consumption of the magnetometer are further reduced, the possibility of the difficult missions, multi-satellite observation, landing on the celestial bodies and exploration of further distant places, would effectively increase. When we try to explore the places where we have not reached, and when the spacecraft is exposed to severe environment, e.g., strong radiation, high and low temperatures, we need to modify the instrument or newly develop techniques, to make the instrument tolerant and keep the good performance. We have to note that new methods sometimes cause disadvantage. For example, when we reduce the size of the sensor core in the fluxgate magnetometer, the noise in the output data generally increases.

Other than the improvement of the magnetometer, good design of the extensible MAST or boom to separate the sensor from the spacecraft is essential for the accurate field measurement. Another important subject for the precise field measurement is the magnetic cleanliness of the spacecraft, reduction of the magnetic interference from every part in the spacecraft to the magnetometer sensor. For the future difficult missions, efforts should be put into these subjects as well as the improvement of the magnetometer.

**Acknowledgments.** The authors wish to express their sincere thanks to all of the BepiColombo MMO MGF team members and JAXA sounding rocket DFG members. We are also grateful to the manufacturing industries of the magnetometers, Sumitomo Heavy

Industries Ltd., Meiwa System Co. and Tierra Tecnica Corporation.

## References

- Acuna, M. H. and N. F. Ness (1976), Results from the GSFC fluxgate magnetometer on Pioneer 11, in *Jupiter: Studies of the Interior, Atmosphere, Magnetosphere and Satellites; Proceedings of the Colloquium*, Tucson, Ariz., May 19–21, 1975 (A77-12001 02-91), edited, pp. 830–847, University of Arizona Press, Tucson.
- Acuna, M. H. and N. F. Ness (1980), The magnetic field of saturn: pioneer 11 observations, *Science*, **207**(4429), 444–446.
- Acuna, M. H., C. S. Scarce, J. B. Seek, and J. Scheifele (1978), The MAGSAT Vector Magnetometer—A Precision Measurement of the Geomagnetic Field, NASA Technical Memorandum, 79656.
- Auster, H. *et al.* (2007), ROMAP: Rosetta Magnetometer and Plasma Monitor, *Space Sci Rev.*, **128**(1), 221–240.
- Auster, H. *et al.* (2008), The THEMIS fluxgate magnetometer, *Space Sci Rev.*, **141**(1), 235–264.
- Baumjohann, W. *et al.* (2010), Magnetic field investigation of Mercury's magnetosphere and the inner heliosphere by MMO/MGF, *Planet Space Sci.*, **58**(1–2), 279–286.
- Benkhoff, J., J. van Casteren, H. Hayakawa, M. Fujimoto, H. Laakso, M. Novara, P. Ferri, H. R. Middleton, and R. Ziethe (2010), BepiColombo Comprehensive exploration of Mercury: Mission overview and science goals, *Planet Space Sci.*, **58**(1–2), 2–20.
- Dougherty, M. K. *et al.* (2004), The Cassini magnetic field investigation, *Space Sci Rev.*, **114**(1–4), 331–383.
- Glassmeier, K.-H. *et al.* (2007), RPC-MAG The Fluxgate Magnetometer in the ROSETTA Plasma Consortium, *Space Sci Rev.*, **128**(1), 649–670.
- Gordon, D. and R. Brown (1972), Recent advances in fluxgate magnetometry, *IEEE Transactions on*, **8**(1), 76–82.
- Gurnett, D. A. (1998), Principles of space plasma wave instrument design, in *Measurement Techniques in Space Plasmas: Fields*, edited by F. Pfaff, E. Borovsky, and T. Young, pp. 121–136, AGU, Washington, D.C.
- Kellock, S. (1996), Cassini dual technique magnetometer instrument (MAG), *Proc. SPIE*, **2803**(1), 141.
- Ness, N. F. (1970), Magnetometers for space research, *Space Sci Rev.*, **11**(4), 459–554.
- Nielsen, O. V. *et al.* (1995), Development, construction and analysis of the 'Ørsted' fluxgate magnetometer, *Measurement Science and Technology*, **6**(8), 1099.
- Pedersen, E. B., F. Primdahl, J. R. Petersen, J. M. G. Merayo, P. Brauer, and O. V. Nielsen (1999), Digital fluxgate magnetometer for the Astrid-2 satellite, *Measurement Science and Technology*, **10**(11), N124.
- Primdahl, F. (1979), The fluxgate magnetometer, *Journal of Physics E: Scientific Instruments*, **12**(4), 241.
- Primdahl, F. (1998), Scalar magnetometers for space applications, in *Measurement Techniques in Space Plasmas: Fields*, edited by F. Pfaff, E. Borovsky, and T. Young, pp. 85–99, AGU, Washington, D.C.

A. Matsuoka (e-mail: matsuoka@isas.jaxa.jp), M. Shinohara, Y.-M. Tanaka, A. Fujimoto, and K. Iguchi